

Research

Green-synthesis of MgO and ZrO₂ nanocomposites: physicochemical properties and antiplasmodial activity in a mouse model

Augustine Innalegwu Daniel^{1,2} · Sarah Udenyi Onogwu³ · Theresa Yebo Gara¹ · Amuda Oladunni⁴ · Jimoh Oladejo Tijani⁵ · Samson Olaitan Oselusi⁶ · Samad Hussein¹ · Hazeedah Mustapha Garba¹ · Aminat Oluwatoyin Salaudeen¹ · Alechine Emmanuel Ameh⁷ · Marshall Keyster⁸ · Ashwil Klein²

Received: 27 December 2024 / Accepted: 28 March 2025

Published online: 23 April 2025

© The Author(s) 2025 [OPEN](#)

Abstract

Malaria remains a significant global health burden, particularly in Sub-Saharan Africa, where drug resistance necessitates novel therapeutic strategies. This study evaluates the antiplasmodial potential of green-synthesized magnesium oxide (MgO) and zirconium oxide (ZrO₂) nanoparticles and their composite (Mg/ZrO₂) using *Eucalyptus camaldulensis* leaf extract. MgO, ZrO₂, and MgO/ZrO₂ nanoparticles were synthesized and characterized using scanning electron microscopy (SEM), transmission electron microscopy (TEM), and X-ray diffraction (XRD), revealing crystalline structures with particle sizes ranging from 39 to 60 nm. Acute toxicity assessment in mice indicated an LD₅₀ > 2000 mg/kg bodyweight, confirming their safety. In vivo antiplasmodial activity was assessed using *Plasmodium berghei*-infected mice, with treatment groups receiving 50, 100, and 200 mg/kg bodyweight each of the nanoparticles. In the suppressive test, MgO-NPs, ZrO₂-NPs, and MgO/ZrO₂-NPs exhibited dose-dependent parasite inhibition of 66.79%, 34.72%, and 41.02% respectively at 200 mg/kg bodyweight. The curative test further confirmed parasite clearance, with MgO-NPs demonstrating the highest efficacy. Nanoparticle treatment also improved survival time and maintained body weight compared to untreated controls. The observed antiplasmodial effects is attributed to enhanced cellular uptake, reactive oxygen species (ROS) generation, and disruption of parasite metabolic pathways. These findings highlight the potential of MgO, ZrO₂ and MgO/ZrO₂ nanocomposites as promising candidates for antimalarial drug development, warranting further mechanistic studies and preclinical validation.

Keywords Antimalaria · Green synthesis · Acute toxicity · *Plasmodium berghei* · Nanotechnology · Malaria

✉ Augustine Innalegwu Daniel, 4112896@myuwc.ac.za; ✉ Alechine Emmanuel Ameh, eameh@uwc.ac.za; ✉ Marshall Keyster, mkeyster@uwc.ac.za; ✉ Ashwil Klein, aklein@uwc.ac.za | ¹Department of Biochemistry, Federal University of Technology, PMB 65, Minna, Niger State, Nigeria. ²Plant Omics Laboratory, Department of Biotechnology, Faculty of Natural Sciences, University of the Western Cape, Robert Sobukwe Road, Bellville 7535, South Africa. ³Department of Chemistry, Joseph Sarwuan Tarka University, PMB 2373, Makurdi, Benue State, Nigeria. ⁴Department of Microbiology, Federal University of Technology, PMB 65, Minna, Niger State, Nigeria. ⁵Department of Chemistry, Federal University of Technology, PMB 65, Minna, Niger State, Nigeria. ⁶DSI/Mintek Nanotechnology Innovation Centre (NIC), Biolabels Node, Department of Biotechnology, Faculty of Natural Sciences, University of the Western Cape, Robert Sobukwe Road, Bellville 7535, South Africa. ⁷Environmental and Nanoscience Group, Department of Chemistry, Faculty of Natural Sciences, University of the Western Cape, Robert Sobukwe Road, Bellville 7535, South Africa. ⁸Environmental Biotechnology Laboratory, Department of Biotechnology, Faculty of Natural Sciences, University of the Western Cape, Robert Sobukwe Road, Bellville 7535, South Africa.



1 Introduction

Malaria is an acute illness caused by *Plasmodium* parasites, which is spread through the bites of infected female *Anopheles* mosquitoes [49]. There are five parasite species that cause malaria namely *P. falciparum*, *P. malariae*, *P. ovale*, *P. knowlesi* and *P. vivax* with *P. falciparum* and *P. vivax* causing the greatest threat to humans [32, 53]. *P. falciparum* is the deadliest malaria parasite and the most prevalent in the African continent [49]. Nigeria, Democratic Republic of Congo, Uganda, Mozambique, Angola, and Burkina Faso accounted for over 90% of malaria cases in Africa, constituting 55% of the global cases [24]. Also, according to WHO 2020 report, over 627,000 deaths occurred globally as a result of malaria out of 241 million malaria-related cases with 77% of these deaths, involving children less than five years of age [24].

Despite efforts by the WHO and other international organisations to eradicate malaria in the world, the disease has continued to be a leading cause of death in Africa particularly Sub-Saharan Africa, where access to medical facilities and medications still remain a big challenge [40]. In 2018, the Commonwealth Leaders agreed to reduce the global cases of malaria by half on or before 2023. Unfortunately, the vision did not materialize due to the COVID-19 pandemic that disrupted global economic growth and distorted the program, leading increased malaria cases and mortality rates. This among other factors clearly shows that the Commonwealth did not achieve its goal [49].

Furthermore, the evolution and spread of parasites resistant to the current available antimalarial drugs is one of the major challenges for effective global malaria control (GMC) [29]. Recently, artemisinin-based combination therapies (ACTs), which are currently the most successful treatments available have played a crucial role in GMC achievement [29]. However, the advent of *P. falciparum* strains partially resistant to artemisinin, primarily recorded in Western Cambodia, Greater Mekong Subregion (GMS) and Southern China poses another threat to these ACTs [48]. The spread of parasites that are resistant to artemisinin (ART) and/or to associated drugs in ACT is a major setback in the treatment of malaria patients and control strategies. Studies have shown that ACT-resistant parasites are responsible for higher failure rate from ACT treatment over the years [12, 20, 45]. Also, the spread of parasite resistant strains from Asia to Africa due to their resistance to antimalarial drugs such as chloroquine and sulfadoxine-pyrimethamine have also frustrated the efforts of malaria eradication around the globe [50]. Although, there have been many concerns about the potential emergence of *k13* mutations linked to artemisinin resistance in Africa, the mutations that have been observed thus far are uncommon and unrelated to *k13* polymorphisms that have been linked to decrease susceptibility in Asia [17, 26, 34, 37]. Therefore, the future of malaria control and global elimination strategies would rely largely on cutting edge research and development of novel chemotherapeutic agents to the next generation of antimalarial drugs [52].

Different parts of plants have been used since ancient times to treat different ailments. The efficacies of plants or its extract as medicinal remedies for ailments is attributed to their phytochemical constituents such as phenols, flavonoids, tannins, alkaloids and saponins [7]. *Eucalyptus camaldulensis*, or Murray Red Gum, is a medicinal plant found in Nigeria, West African countries, Asia and Australia (Sebei et al. 2015). The plant has been used by the locals or traditional herbalist to treats different ailments such as microbial infection, wound healing, aches, respiratory diseases and malaria [2]. For instance, the leaf is used among the Igala people of Kogi State in Nigeria to treat malaria and fever [2, 11]. According to Aljawdah et al. [4], treatment of mice with *E. camaldulensis* extract inhibited 9.4% malaria parasites in mice. The antimalaria activity of the extract was attributed to the presence of phenols and flavonoids which were the major phytoconstituents identified in the extract. Also, Dkhil et al. [18] reported that leaf extract of the plant suppresses about 84% of *Plasmodium* parasites which was attributed to the phytoconstituents of the plant.

There are different strategies and methods available for developing novel antimalarial drugs, some of which have been derived from biological materials such as plants, animals, and microorganisms [29]. Recently, nanotechnology, which is an emerging field of science with wide applications in diverse field of human endeavours, have offered a new approach to the development of novel therapeutic drugs for the management of diseases [40]. Different studies have shown that biological methods of synthesis of nanomaterials are a promising alternative to the conventional chemical methods [10, 30, 56]. Studying the physical and chemical properties of nanomaterials for biomedical applications is essential because it provides the connection between their biological activity with specific parameters such as composition, size, shape, and capping [10]. Also, size as well as surface properties of nanomaterials are an important criterion to determine their pharmacokinetic, bioavailability, and biological activity [56]. The potential of nanomaterials to provide controlled-release of active materials/ingredients is advantageous to address recrudescence, which is frequently encountered during artemisinin-based therapy [44]. The use of nanomaterials has been reported to

enhance treatment results and efficacies due to their unique properties such as large surface area and morphology, size distribution, catalytic properties, high conductivity and stability, and the ability to manipulate them to carry out a desired function in the biological system such as functionalization for active targeting of cells or organs [55].

Metallic nanoparticles are useful and safe in nature, with many applications in biomedical and agricultural research, electronics, cosmetics, food, and environmental remediation [3, 28]. The biological uses of metallic nanoparticles such as zinc oxide, iron oxide, silver, and titanium nanoparticles include as antibacterial [42, 43], antifungal [8, 33], and antiviral agents [15, 39]. In vivo antiplasmodial study of magnesium oxide nanoparticles (MgO-NPs) and zirconium oxide nanoparticles (ZrO₂-NPs) are scanty in literature. Other metallic nanoparticles such as silver (Ag) and zinc oxide (ZnO) nanoparticles have been used in vitro for their antiplasmodial potential. In a study by Najoom et al. [38], ZnO nanoparticles significantly inhibited *Plasmodium* parasites with lower doses, while Hawadak et al. [23] showed that silver nanoparticles inhibited *Plasmodium* parasites with less haemolysis of the red blood cells. Currently, there is no study on the antiplasmodial activity of metallic nanocomposites. Previous studies only report on the antiplasmodial activity of individual metallic nanoparticles. This is the first study to explore the antiplasmodial activity of MgO/ZrO₂-NPs in *P. berghei* infected mice. Therefore, the aim of this study is to evaluate the antiplasmodial potentials of phyto-mediated magnesium and zirconium oxide (ZrO₂) nanocomposite against chloroquine sensitive NK-65 *P. berghei* infected albino mice. The objectives of the study include synthesis and characterization of the nanomaterials, acute toxicity testing and evaluation of in vivo antiplasmodial activity of the nanomaterials using suppressive and curative test.

2 Materials and methods

2.1 Materials

Fresh leaves of *Eucalyptus camaldulensis* were collected from Bosso Campus of Federal University of Technology, Minna, Niger State, Nigeria. The leaves were identified and authenticated at the Plant Biology Department of Federal University of Technology Minna and assigned a voucher number: FUT/PLB/MYR/001. The leaves were washed with clean water and air dried at the Laboratory of Biochemistry Department for 2 weeks to a constant dried weight. Zirconium tetrachloride octahydrate (ZrCl₄·8H₂O) ≥ 99.5%, magnesium sulfate heptahydrate (MgSO₄·7H₂O) ≥ 98% and sodium hydroxide ≥ 97% were used for the synthesis of MgO-NPs, ZrO₂-NPs and MgO/ZrO₂-NPs.

2.2 Methods

2.2.1 Preparation of plant extracts

The dried leaves were blended into fine powder using a kitchen blender, and 20 g of the powder was extracted with 400 mL of distilled water at 45 °C for 30 min using a magnetic stirrer to obtain a concentration of 50 mg/mL. The extract was filtered using a muslin cloth and centrifuged to obtain a fine filtrate, which was preserved in the refrigerator at 4 °C.

2.2.2 Synthesis of magnesium oxide nanoparticle (MgO-NPs) and zirconium oxide nanoparticle (ZrO₂-NPs)

The synthesis of MgO-NPs or ZrO₂-NPs was carried out following the reported protocol of Khan et al. [27] and Chau et al. [16] with slight modifications. Exactly 20 mL of the plant extract and 100 mL of 0.2 mM solution of either magnesium sulphate or zirconium tetrachloride was stirred continuously on a magnetic stirrer for 2 h at 60 °C. The pH of the mixture was adjusted to 9 using 0.2 M NaOH and stirred further for another 1 h. The synthesis of the nanoparticles was confirmed by a colour change from light green to milky colour for MgO-NPs and light green to yellow for ZrO₂-NPs. The solution was immediately centrifuged to collect the nanoparticles which was washed severally with deionized water to remove any trace of impurities. The nanoparticles were oven dried at 60 °C to a powdered form and calcined at 500 °C for 3 h.

2.2.3 Synthesis of magnesium oxide/zirconium oxide nanocomposite (MgO/ZrO₂-NPs)

For the synthesis of MgO/ZrO₂-NPs, 50 mL each of 0.2 mM solution of MgSO₄ and ZrCl₄·8H₂O solution were combined and stirred continuously for 30 min. This was followed by the addition of 20 mL of the plant extract before stirring for 3 h. The pH of the solution was adjusted to 9 using 0.2 M NaOH and stirred further for another 1 h. The synthesis of the

nanoparticle was confirmed by colour change from light green to grey black. The solution was immediately centrifuged, washed severally with deionized water to obtain the synthesized nanoparticles in pellet form. The pellet was oven dried overnight at 60 °C and calcined at 500 °C for 3 h.

2.2.4 Characterization of the nanoparticles

The synthesized nanoparticles were preliminarily characterized using scanning and transition electron microscope (SEM and TEM) (Zeiss Aunga) to determine the size and morphology of the nanoparticles. Powder X-ray diffractometer (Bruker d8) was used to acquire the X-ray diffraction (XRD) patterns of the synthesized nanoparticles and to determine the crystallinity of the nanoparticles using the Derby Sherer equation:

$$L = \frac{K\lambda}{FWHM \times \cos\theta}$$
 where L is the crystallite size, K is the constant, which is equivalent to 0.94, $\lambda = 1.54178$ and θ is the peak position in radian.

2.2.5 Experimental animals

A total of 75 albino mice of 6–7 weeks old and weighing between 18 and 25 g of both sexes were used for this study. The mice were obtained from the animal house of the Veterinary Department of the University of Jos, Nigeria. The mice were kept in well-ventilated metal cages and maintained at room temperature of 25 ± 2 °C, 45–55% of relative humidity on a 12 h light/12 h dark cycle, with access to water and pelletized standard guinea feed *ad libitum*. The mice were kept for 21 days to acclimatize to the environmental conditions. Ethical approval for the animal studies was obtained from the Directorate of Research, Innovation and Development (Animal Ethics Committee), Federal University of Technology, Minna, Nigeria (000079). To minimize pain and discomfort, the mice were monitored daily for any symptoms resulting from the treatment. At the end of each experiment, mice were euthanized by intraperitoneal injection of 160 mg/kg sodium pentobarbital.

2.3 Acute toxicity testing of the nanoparticles

Oral acute toxicity test of the nanoparticles was carried following the standard guidelines of the Organisation for Economic Co-operation and Development (OECD) as described by Misganaw et al. [35]. For a sighting study, a single dose of 2000 mg/kg bodyweight (bwt) each of MgO-NPs, ZrO₂-NPs, and MgO/ZrO₂-NPs were separately administered to a mouse by oral gavage. Since no mortality was recorded within 24 h, an additional four mice each were used and administered the same dose of the nanoparticles and distilled water was administered to the normal control. The mice were monitored continuously every 30 min for 4 h and then daily for the next 14 days for the general signs and symptoms of toxicity.

2.4 *P. berghei* parasites

A chloroquine sensitive strain of *P. berghei* (NK-69) was obtained from the National Institute of Medical Research (NIMER), Yaba Lagos, Nigeria and was maintained by sub-passage in mice.

2.5 Parasite inoculation

The parasite was inoculated intraperitoneally into the mouse with 0.2 mL of infected blood containing about 1×10^7 *P. berghei*-parasitized erythrocytes. The inoculum consists of 5×10^7 *P. berghei* erythrocytes per mL. This was prepared by determining both the percentage parasitaemia and the erythrocytes count of the donor mouse under light microscope and diluting the blood with isotonic normal saline in ratio indicated by both determinations [31].

2.6 Drug administration

Artemether/lumefantrine (Art/Lum) was used as the positive control in this study. The drug, MgO-NPs, ZrO₂-NPs, and MgO/ZrO₂-NPs used for the antiplasmodial study were administered orally using a stainless metallic feeding cannula.

2.7 In vivo antiplasmodial activity of the nanoparticles

2.7.1 Evaluation of Peters' 4-day suppressive test of the nanoparticles

This study evaluated the schizontocidal effects of the nanoparticles and artemether/lumefantrine against early-stage *P. berghei* infection in mice using Peters' 4-day suppressive assay. Twenty-five Swiss albino mice were infected with the parasite on the first day and randomly divided into five groups, each containing five mice. The treatment groups were administered nanoparticles at oral doses of 50, 100, and 200 mg/kg bodyweight, while another group received Art/Lum (1.4 mg/kg bodyweight). The control group was given distilled water. On the fifth day, thin blood smears were prepared from tail blood samples, stained with Giemsa, and examined under a microscope to count the number of infected erythrocytes out of 500 randomly observed cells [31]. The average percentage reduction in parasitaemia was calculated in comparison with the control group using the following formula:

$$\% \text{ suppression} = \frac{\text{Mean \% parasitaemia in the negative control group} - \text{Mean \% parasitaemia in the treated group}}{\text{Mean \% parasitaemia in the negative control group}} \times 100$$

2.8 Evaluation of curative activities of the nanoparticles (Rane's test)

This study assessed the schizontocidal activity of the nanoparticles and artemether/lumefantrine in mice with established infections, following the method outlined by Ryley and Peters [46]. On the first day, *P. berghei* was injected intraperitoneally into 25 mice. After 72 h, the mice were randomly divided into five groups, each containing five animals. Groups I to III received oral doses of the nanoparticles at 50, 100, and 200 mg/kg bodyweight, respectively. Group IV (positive control) was treated with Art/Lum at 1.4 mg/kg body weight, while Group V (negative control) was given distilled water. The treatments were administered once daily for seven days. To monitor the parasitaemia levels, Giemsa-stained thin blood smears were prepared from tail blood samples every two days during the treatment period. Additionally, changes in body weight and packed cell volume (PCV) were recorded every two days throughout the experiment.

2.9 Data analysis

The data generated from this study were analysed using GraphPad Prism software (version 9.0.0 for Windows). Study results were presented as the mean \pm standard error of the mean (SEM). To compare group outcomes, a one-way ANOVA was performed, followed by Duncan's post-hoc test for multiple comparisons. A p-value of < 0.05 was considered statistically significant at a 95% confidence level.

3 Results and discussion

3.1 Characterization of phyto-mediated nanoparticles

The synthesis of MgO-NPs, ZrO₂-NPs, and MgO/ZrO₂-NPs was conducted via green route. Scanning and transmission electron microscopy (SEM and TEM) analysis of the nanoparticles shows that MgO-NPs were spherical, agglomerated and monodispersed with distinct particle sizes (Fig. 1a and b), while ZrO₂-NPs were oval shape and agglomerated with compacted particle grains (Fig. 1c and d). There was a mixture of spherical and oval shape particles in MgO/ZrO₂-NPs. The particles are compacted and agglomerated with no distinct separation between the grains of the nanomaterials (Fig. 1e and f). The agglomeration of the nanomaterials might be due to the electrostatic or van der Waal force of attraction resulting from the metallic elements used for the synthesis. This attraction was even more evident in the nanocomposite (Fig. 1e) creating a hollow pore at the core of the nanomaterials. According to Arsuaga et al. [9], agglomeration of nanomaterials due to attractive van der Waals forces can give rise to inhomogeneities and defects in their morphology.

Particle size analysis of the nanomaterials shows that MgO-NPs contains particles ranging between 20 and 80 nm with an average particle size of 42.71 ± 11.60 nm (Fig. 2a), ZrO₂-NPs contains particles ranging between 30 and 100 nm with an average particle size of 60.22 ± 6.54 nm (Fig. 2b) while MgO/ZrO₂-NPs contains particles ranging from 20 to 70 nm with

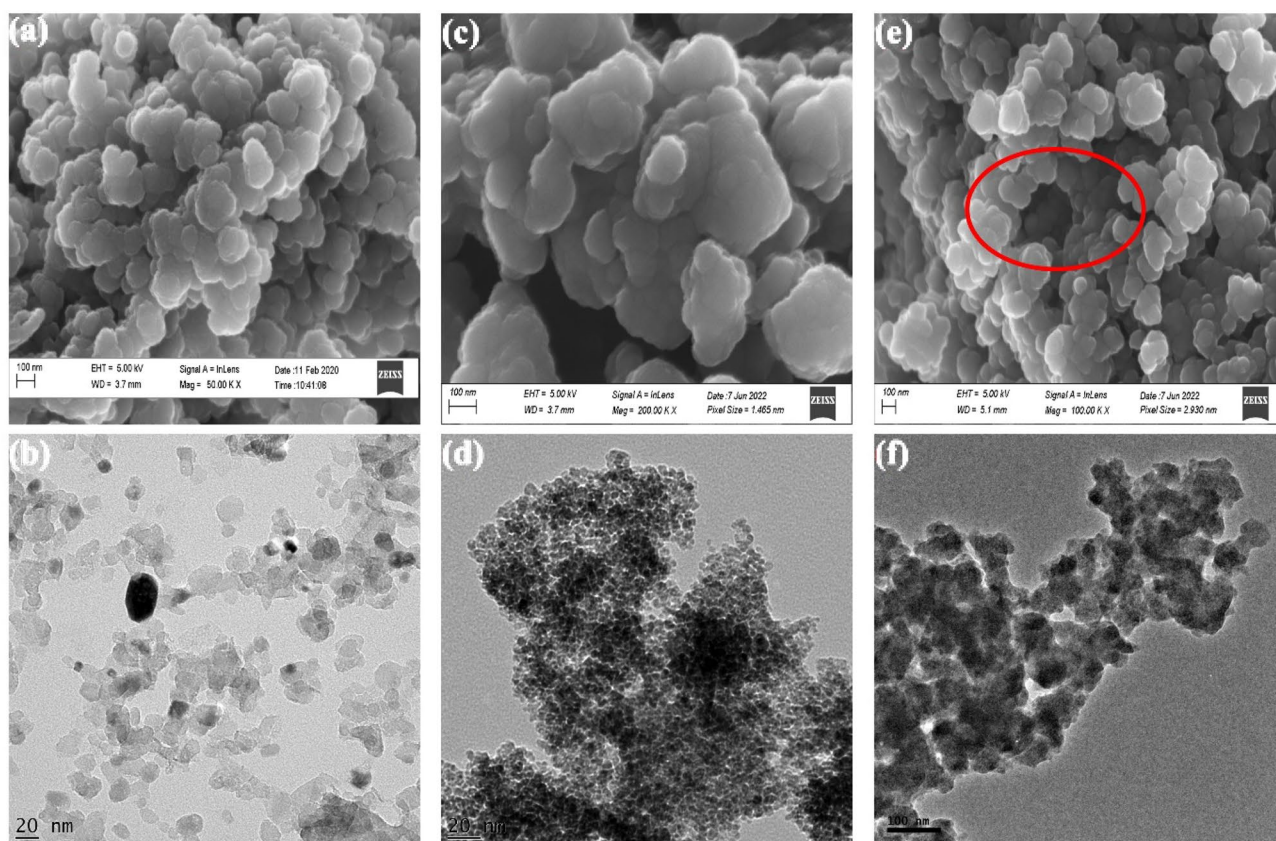


Fig. 1 SEM and TEM images of metallic (a and b) MgO-NPs, (c and d) ZrO₂-NPs and (e and f) MgO/ZrO₂-NPs respectively synthesized using extract of *E. camaldulensis*. The SEM image of MgO/ZrO₂-NPs shows a hollow pore (red circle) at the centre of the nanomaterials, which can be attributed to the attraction force between the metallic Mg and Zr present in the nanomaterials

an average particle size of 39.25 ± 9.80 nm (Fig. 2c). The particle size of MgO-NPs and ZrO₂-NPs reported in this study is higher than 11.68 and 5 nm particle size reported by Ammulu et al. [5] and Kumaresan et al. [30] respectively for MgO-NPs and ZrO₂-NPs. The differences in the particle sizes maybe due to the concentration of the metallic salts and capping agents used and the synthesis condition [51]. Also, it has been reported that the particle size of ZrO₂-NPs ranges between 5 and 150 nm but particle size less than 50 nm are usually obtained when chemical or biological synthesis methods is used [51]. Finally, Amrulloh et al. [6] reported a particle size range between 60 and 100 nm for MgO-NPs synthesized using *Mangifera indica* bark.

Elemental analysis of the nanomaterials shows the presence of the constituent elements (Mg, Zr, and O) in different proportions. In MgO-NPs, there was 41.4% O and 50.69% Mg while ZrO₂-NPs contain 51.4% O and 43.35% Zr. For MgO/ZrO₂-NPs, the nanomaterials contain 20.51%, 33.89% and 39.34% of Mg, Zr and O respectively (Table 1). All the nanomaterials contain small amount of carbon (C), which may be contributed by the plant materials used as a reducing or capping agent during the synthesis. The presence of C in the nanomaterials may also be due to the bioactive metabolites of *E. camaldulensis*, which play a dual role in both reducing and stabilizing the nanomaterials [1]. According to Shayoub et al. [47] and Ghareeb et al. [19], leaf extract of *E. camaldulensis* contains phytochemicals such as flavonoids and phenols, which has been reported to be a good capping and reducing agents for the synthesis of nanoparticles.

X-ray diffraction analysis of the nanoparticles shows the appearance of different diffraction peaks in all the nanomaterials with different fragmentation patterns and distinct phases (Fig. 3). In MgO-NPs, the periclase and lattice face-centred cubic nanomaterial shows the appearance of peaks at position 36.94°, 42.92°, 62.30°, 74.69° and 78.63° with a fragmentation pattern of (111), (200), (220), (311) and (222), respectively and a crystallite size of 11.69 ± 0.23 nm. Monoclinic tetragonal ZrO₂-NPs shows the presence of similar peaks with MgO/ZrO₂-NPs at position 30.22°, 34.57°, 50.22° and 59.28° with a fragmentation pattern of (101), (002), (112) and (103) with a crystallite size of 4.16 ± 0.82 and 6.07 ± 0.51 nm for ZrO₂-NPs and MgO/ZrO₂-NPs, respectively. There was an emergence of unidentified peak at position 50.22° and 60.00° in MgO-NPs, which becomes prominent in MgO/ZrO₂-NPs while

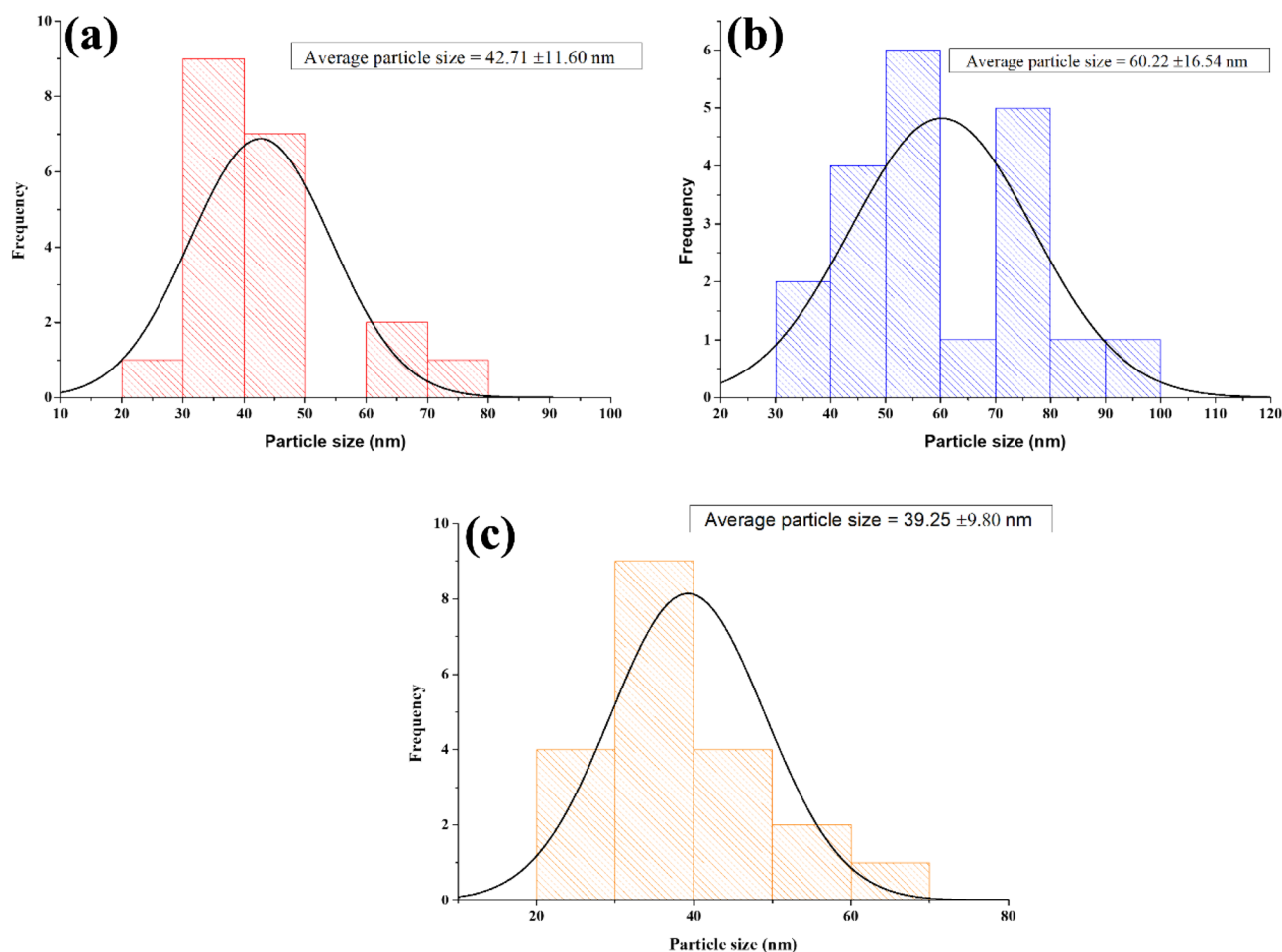


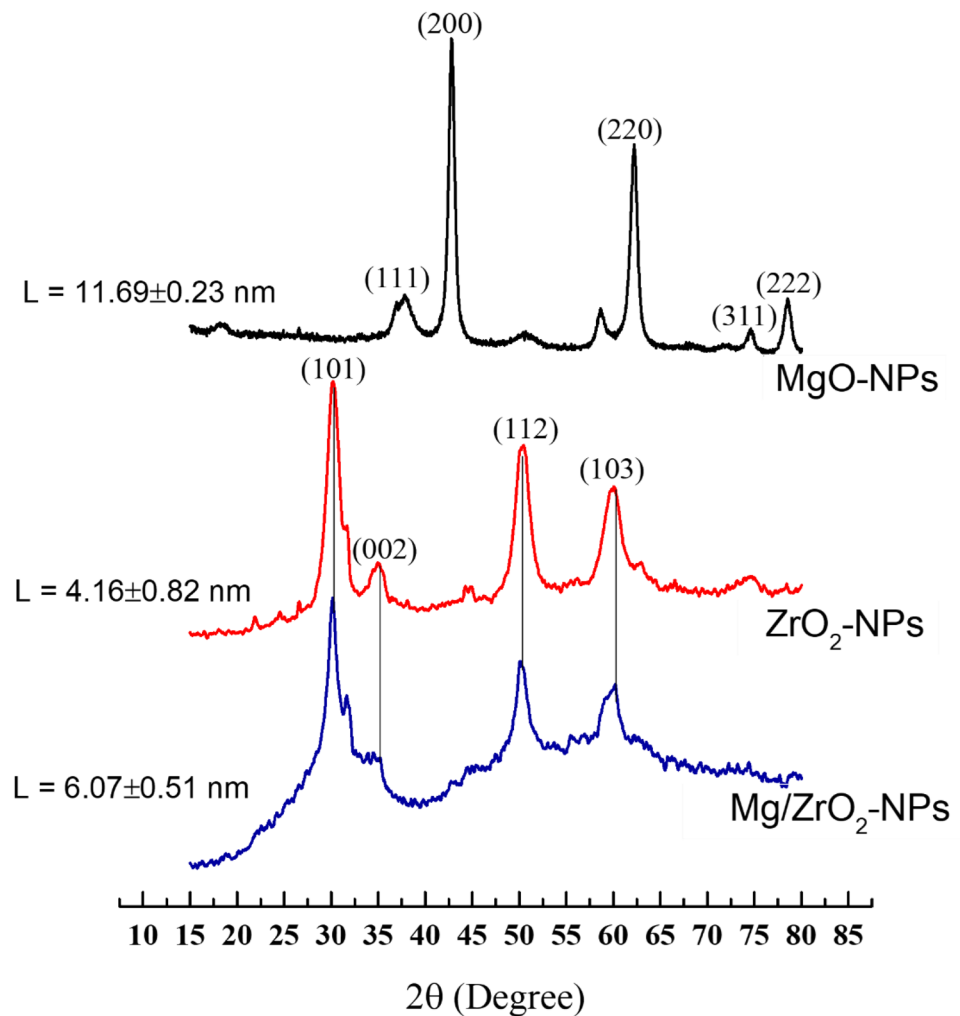
Fig. 2 Particle size distribution of (a) MgO-NPs, (b) ZrO₂-NPs and (c) MgO/ZrO₂-NPs synthesized using extract of *E. camaldulensis*

Table 1 Elemental composition of the metallic nanoparticles synthesized using extract of *E. camaldulensis*

Elements	MgO-NPs	ZrO ₂ -NPs	MgO/ZrO ₂ -NP
C	7.91	5.25	6.26
O	41.4	51.4	39.34
Mg	50.69	–	20.51
Zr	–	43.35	33.89
Total	100.00	100.00	100.00

peaks at position 74.69° and 78.63° which are prominent in MgO-NPs where absent in MgO/ZrO₂-NPs (Fig. 3). Studies have shown that increase crystallite size increases with increasing temperature and reaction time [22, 54]. From this study, a temperature of 60°C and 3 h reaction time was chosen based on the reported optimal condition for the synthesis of these nanomaterials in literature [36]. Crystallite size is one of the important parameters that influence physical properties of nanomaterials. Crystallite size is inversely proportional to the surface area of material [54]. Therefore, the synthesized nanomaterials shows that ZrO₂-NPs have more surface area followed by MgO/ZrO₂-NPs and MgO-NPs. Finally, the diffraction peaks pattern is similar to those identified by Younis et al. [56] who synthesized MgO-NPs using *Rosa floribunda* charisma extract and Bishwokarma et al. [14] for ZrO₂-NPs synthesized using *Curcuma longa* extract.

Fig. 3 X-ray diffraction pattern of MgO-NPs, ZrO₂-NPs and MgO/ZrO₂-NPs synthesized using extract of *E. camaldulensis*



3.2 Acute oral toxicity test of the nanoparticles

Acute oral toxicity test shows that the nanoparticles (MgO-NPs, ZrO₂-NPs, and MgO/ZrO₂-NPs) did not cause any gross behavioural changes and mortality within 24 h as well as in the following days, indicating that the LD₅₀ values of the nanoparticles is greater than 2000 mg/kg body weight in mice as per OECD 423 guidelines [13]. The mice show no loss of appetite and weakness in the first hour of administration of the nanoparticles with normal breathing, eye colour, skin, and fur position throughout the study period. Therefore, 50, 100, and 200 mg/kg bodyweight doses of the nanomaterials were selected for antiplasmodial study.

3.3 Antiplasmodial activity of the nanoparticles

Peter's 4 days suppressive study of the nanoparticles shows a dose-dependent suppression of the parasites (Table 2). MgO-NPs at 50, 100, and 200 mg/kg bodyweight significantly inhibited 38.54 ± 3.91 , 55.34 ± 2.60 , and $66.79 \pm 2.05\%$ of the parasites. The level of parasite inhibition by ZrO₂-NPs and MgO/ZrO₂-NPs was not significantly different ($p > 0.05$) at 50 and 100 mg/kg bodyweight doses but at 200 mg/kg bodyweight, MgO/ZrO₂-NPs show a slightly higher inhibition of the parasites compared to ZrO₂-NPs (Table 2). This result was further confirmed using the Rane's curative

Table 2 Percentage parasite suppression by metallic nanoparticles synthesized using extract of *E. camaldulensis*

Nanoparticles	% Suppression			Art/Lum (1.4 mg/kg bwt)*
	50 mg/kg bwt	100 mg/kg bwt	200 mg/kg bwt	
MgO-NPs	38.54 ± 3.91 ^a	55.34 ± 2.60 ^b	66.79 ± 2.05 ^c	90.07 ± 0.66 ^d
ZrO ₂ -NPs	29.76 ± 5.97 ^a	31.21 ± 3.28 ^b	34.72 ± 3.33 ^b	90.07 ± 0.66 ^c
Mg/Zr-NPs	29.76 ± 3.23 ^a	31.86 ± 2.36 ^b	41.023.44 ^c	90.07 ± 0.66 ^d
Negative control	0	0	0	0

Values are expressed in mean ± standard error of mean of 5 replicates. Values with the same superscript alphabet on the same column have no significance difference at $p < 0.05$. Bwt = Bodyweight. * Serve as the positive group (group treated with 1.4 mg/kg bwt of Artemether/lumefantrine)

test. The nanoparticles show a significant dose-dependent clearance of the parasites from the erythrocytes of the mice, which was comparable to the standard drug (artemether/lumefantrine) used as positive control. The observed antiparasitic activity of the nanoparticles can be attributed to their particle and crystallite sizes. Smaller particle size will have a larger surface area and will have more penetration into the cells resulting in more efficient interaction with the parasites. Also, the high surface-volume ratio of this smaller nanoparticles will lead to a significant release of reactive oxygen species that can alter the cellular structure of the parasite [21]. The crystallite sizes of the nanoparticles may lead to higher surface energy, which can enhance the interaction between the nanoparticles and the biological membrane of the parasite resulting in a better antiparasitic effect [41]. Furthermore, according to Adesida et al. [2], 800 mg/kg bodyweight of leaf extract of *E. camaldulensis* suppresses 53.69% *P. berghei* parasite and a curative effect of 81.26%. Also, Kabiru et al. [25] treated mice with 100, 200 and 400 mg/kg bodyweight aqueous and methanolic extract of *E. camaldulensis*. Their results show a significant decrease ($p < 0.05$) in the parasitaemia level of mice by the methanol extract. These studies support the findings reported in this study and justify the choices of our doses used for this study. The antimalarial properties of the nanomaterials stem from multiple mechanisms, including direct parasite suppression, oxidative stress induction, and enhanced cellular interactions. Their small size (39–60 nm) and high surface energy likely enhance their penetration into red blood cells, disrupting parasite metabolic pathways. Additionally, the nanoparticles may generate reactive oxygen species (ROS), causing oxidative damage to *Plasmodium* parasites and leading to cell death. Their crystallite structure further facilitates interaction with the parasite's biological membrane, improving efficacy. While not explicitly analysed, immune modulation could also play a role in their antiparasitic activity. These findings highlight the potential of these nanomaterials as novel antimalarial agents, warranting further studies on their molecular interactions, long-term safety, and efficacy against drug-resistant strains (Fig. 4).

3.4 Effect of the nanoparticle's treatment on the packed cell volume (PCV), bodyweight changes and mean survival time of the mice

Treatment of the mice with different doses (50, 100, and 200 mg/kg bodyweight) of the nanoparticles shows a significant change ($p < 0.05$) in the PCV of the mice compared to group treated with 1.4 mg/kg bodyweight of artemether/lumefantrine (Fig. 5). The negative control group show a significant change ($p < 0.01$) in the bodyweight of the mice with a significant drop on the 8th days of the study (Fig. 5). Furthermore, the nanomaterials had no significant effect on the bodyweight of the mice throughout the period of treatment (Fig. 6). There was no significant change in the bodyweight of mice treated with the different doses of the nanoparticles between the first 3 days (Fig. 6) however, on the 8th day, there was a significant change in the bodyweight of the mice particularly the negative control group, which shows a significant drop in the bodyweight of the animals. The different doses of the nanoparticles were able to averagely maintain the bodyweight of the mice throughout the treatment period compared with the positive control group. Treatment with different doses of the nanoparticles was also able to extend the survival time of the mice in a dose-dependent manner compared to the negative control group which have a mean survival time below 10 days (Fig. 7). The negative control

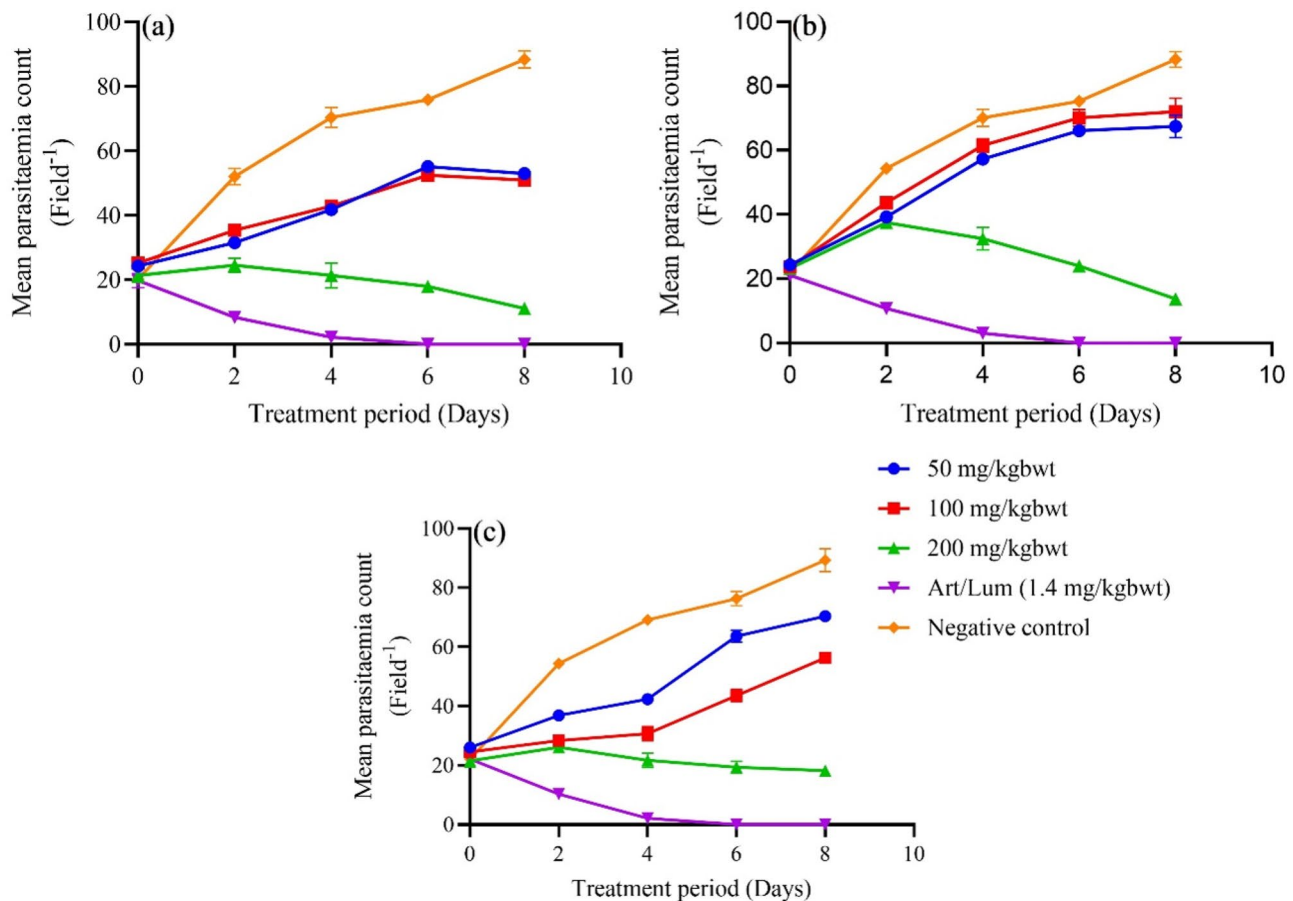


Fig. 4 Effect of phyto-mediated metallic nanoparticles on the mean parasitaemia level of mice infected with *P. berghei* parasites and treated with 50, 100, and 200 mg/kg bodyweight of (a) MgO-NPs, (b) ZrO₂-NPs, and (c) MgO/ZrO₂-NPs. The control group was administered Art/Lum (1.4 mg/kg bodyweight) while negative control group consist of mice infected with the parasite and left untreated throughout the period of the study. Bwt = Bodyweight

group, which was infected with the *Plasmodium* parasite but not treated show a significant decrease ($p < 0.05$) in their bodyweight because of the parasites. During malaria infection, loss of appetite is a preliminary symptoms, which affect the feeding behaviour of the patient. From the acute toxicity study, the nanomaterials had no effect on the feeding behaviour of the mice hence maintenance of their bodyweight during the treatment period. Finally, treatment with different doses of the nanoparticles was found to extend the survival time of the mice compared with the negative control group (Fig. 7). This is an indication that the nanoparticle was able to reduce the virulence of the parasite and hence prevent the mortality of the mice (Fig. 7). In the negative control group, the mice were able to withstand the virulence of the parasite for about 8–9 days and majority of the mice died after 8 days because of the increase in the number of parasites in their erythrocytes.

4 Conclusion

The result from this study shows the successful synthesis of MgO-NPs, ZrO₂-NPs and MgO/ZrO₂-NPs using leaf extract of *E. camaldulensis*. Antiplasmodial activity of the nanoparticles at different doses shows a significant inhibition of the parasites in a dose-dependent manner with moderate effect on the PCV and bodyweight changes of the mice. The treatment also shows a significant increase in the survival time of the *P. berghei* infected mice compared with the negative control

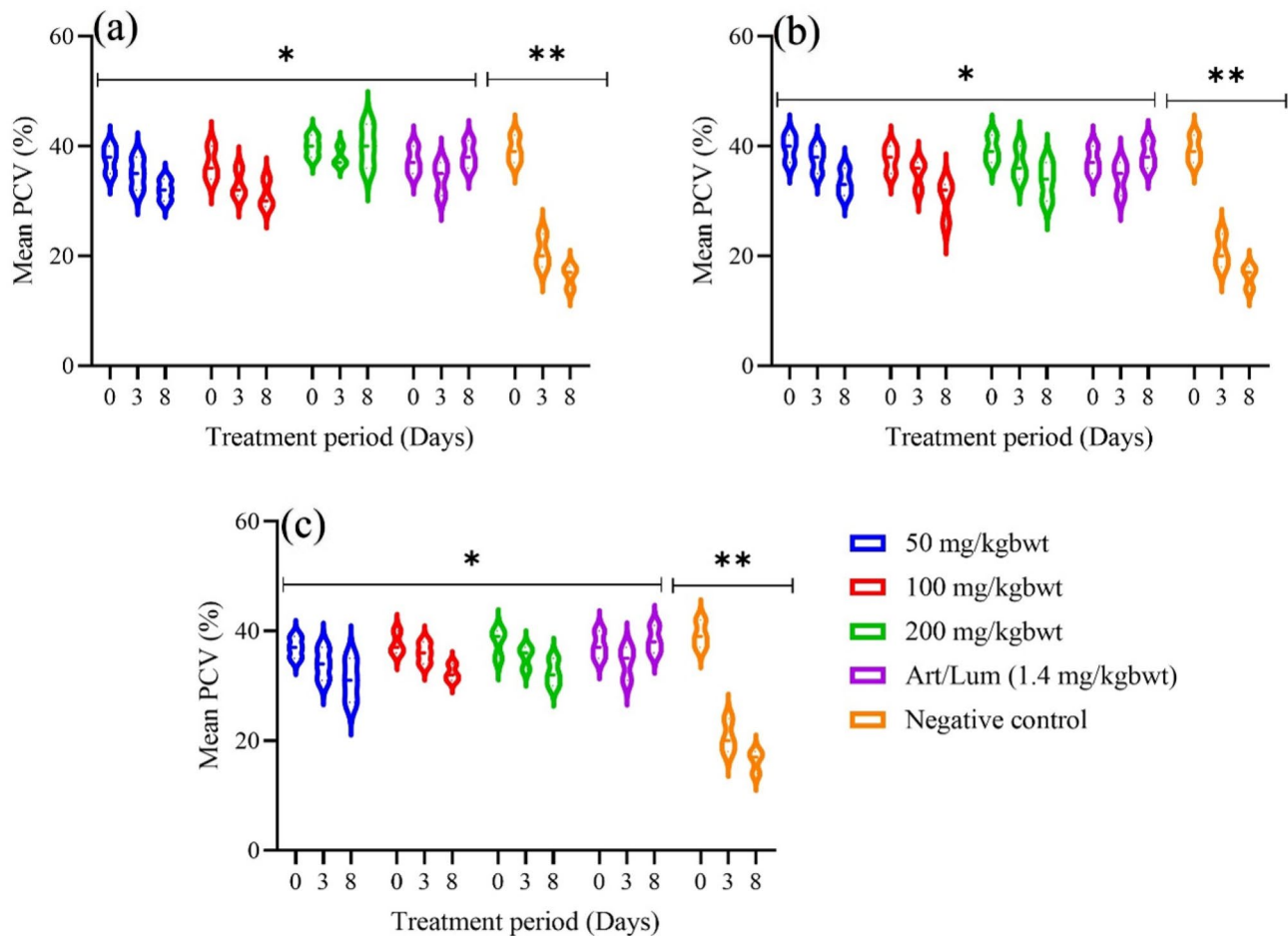


Fig. 5 Effect of phyto-mediated metallic nanoparticles on packed cell volume (PCV) of *P. berghei*-infected mice. Mice were treated with 50, 100 and 200 mg/kg bwt of (a) MgO-NPs, (b) ZrO₂-NPs and (c) MgO/ZrO₂-NPs for a period of 7 days. The control group was administered Art/Lum (1.4 mg/kg bwt) while negative control group consist of mice infected with the parasite and left untreated throughout the period of the study. Violin with * shows statistically significant difference at $p < 0.05$ while violin with ** were statistically significant at $p < 0.01$. bwt=Bodyweight

mice with shorter survival time. This study therefore shows that the synthesis nanoparticles maybe a good candidate compound for the formulation of chemotherapeutic drug to control malaria parasites infections.

4.1 Limitation and future directions

This study has some limitations, including its focus on *P. berghei* infected mice, which may not fully represent human malaria infections, necessitating further validation in higher animal models and clinical trials. Additionally, while acute toxicity was assessed, long-term toxicity, including chronic, genotoxic, and immunotoxic effects, remains unexplored. The precise mechanism of action of the nanoparticles, such as their impact on parasite metabolic pathways and host immune responses, was not fully characterized. Moreover, nanoparticle stability, pharmacokinetics, and bioavailability were not investigated, which are crucial for clinical translation. Future research should focus on optimizing nanoparticle formulations through surface functionalization or drug conjugation, conducting in-depth mechanistic studies on their mode of action, evaluating chronic toxicity and biodistribution, and testing their efficacy against drug-resistant *Plasmodium* strains. Ultimately, further preclinical studies, including primate models and potential human trials, will be necessary to establish the therapeutic potential of these nanoparticles as next-generation antimalarial agents.

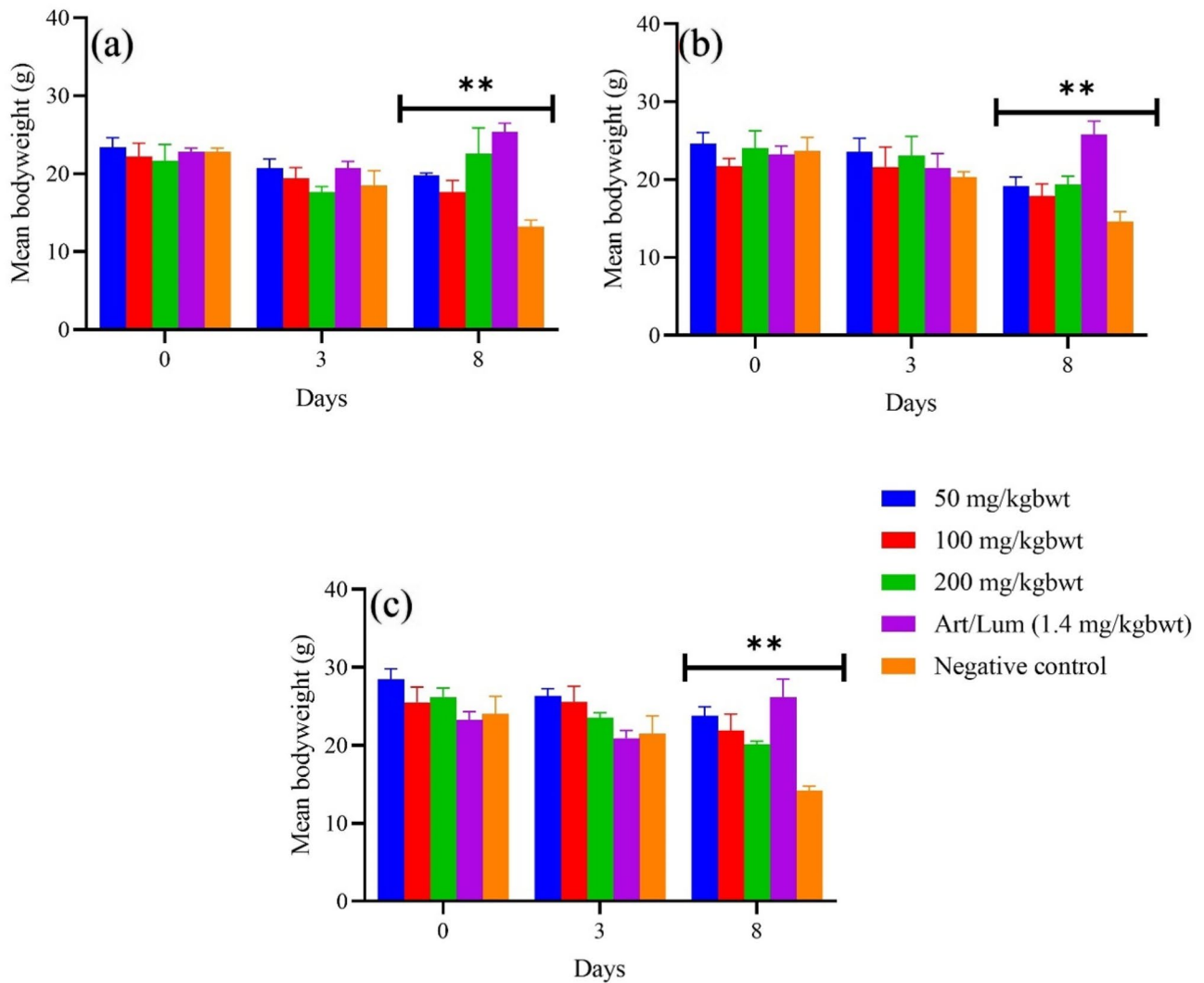
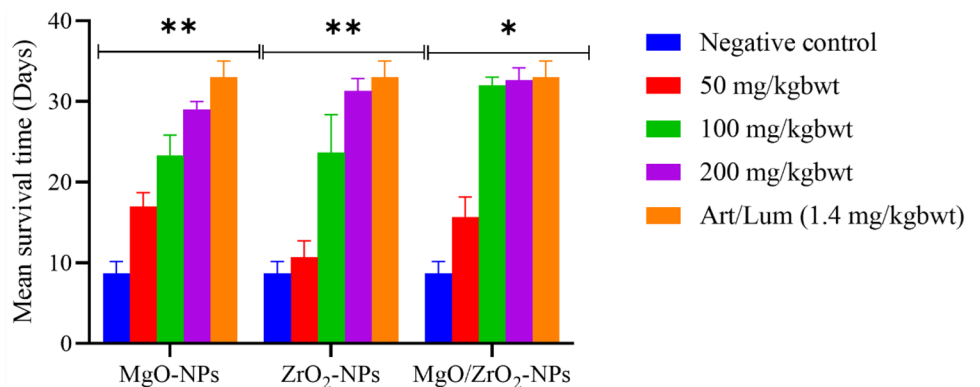


Fig. 6 Effect of phyto-mediated metallic nanoparticles on the mean bodyweight of *P. berghei* infected mice. Mice were treated with 50, 100 and 200 mg/kg bodyweight of (a) MgO-NPs, (b) ZrO₂-NPs and (c) MgO/ZrO₂-NPs for a period of 7 days. The control group was administered Art/Lum (1.4 mg/kg bwt) while negative control group consist of mice infected with *plasmodium* parasite and left untreated throughout the period of the study. Bars with ** shows statistically significant difference at p<0.05. bwt = Bodyweight

Fig. 7 Mean survival time of mice treated with different doses (50, 100 and 200 mg/kg bwt) of MgO-NPs, ZrO₂-NPs, MgO/ZrO₂-NPs and Art/Lum (1.4 mg/kg bwt). Negative control group consist of mice infected with the parasite and left untreated throughout the period of the study. Bars with * are significantly different at p<0.05 while bars with ** are significantly different at p<0.01. bwt = Bodyweight



Authors contributions A.I.D, J.O.T, M.K, A.K and A.E.A: Project conceptualization, design, supervision, and administration. S.U.O, T.Y.G A. O and S.O: Writing, editing, analysis, and Manuscript draft. H.M.G, S. H, A.O.S: Writing, review and editing. A.I.D: Data curation and validation. All authors reviewed the manuscript.

Funding This research did not receive funding from any source.

Data availability Data is provided within the manuscript.

Declarations

Ethics approval and consent to participate This study was approved by the Research Ethics Committee, Federal University of Technology, Minna, Niger State, Nigeria. Assigned number: 000079. Not applicable.

Consent for publication All the authors have given consent for publication of manuscript.

Competing interests The authors declare no competing interests.

Plant guidelines The authors confirm that the use of plant in the present study complies with international, national and/or institutional guidelines.

Permissions to collect the plants/plant parts The plant specimen was collected with permissions.

Source of the plant used in your study The plant name and the source is in the Methods section.

Open Access This article is licensed under a Creative Commons Attribution-NonCommercial-NoDerivatives 4.0 International License, which permits any non-commercial use, sharing, distribution and reproduction in any medium or format, as long as you give appropriate credit to the original author(s) and the source, provide a link to the Creative Commons licence, and indicate if you modified the licensed material. You do not have permission under this licence to share adapted material derived from this article or parts of it. The images or other third party material in this article are included in the article's Creative Commons licence, unless indicated otherwise in a credit line to the material. If material is not included in the article's Creative Commons licence and your intended use is not permitted by statutory regulation or exceeds the permitted use, you will need to obtain permission directly from the copyright holder. To view a copy of this licence, visit <http://creativecommons.org/licenses/by-nc-nd/4.0/>.

References

1. Abdel-Aziz MM, Emam TM, Elsherbiny EA. Bioactivity of magnesium oxide nanoparticles synthesized from cell filtrate of endobacterium *Burkholderia rinojensis* against *Fusarium oxysporum*. *Mater Sci Eng, C*. 2020;109: 110617.
2. Adesida SA, Oguntimehin SA, Famuyiwa FG, Faloye KO, Ogundele SB, Bello OI, Oladiran OJ, Olusola AJ, Adewole AH, Adebayo PA. Larvicidal and antiplasmodial studies of *Eucalyptus camaldulensis* (Myrtaceae) Leaf. *Adv Tradit Med*. 2024;24:1169–79.
3. Ahmed S, Ahmad M, Swami BL, Ikram S. A review on plants extract mediated synthesis of silver nanoparticles for antimicrobial applications: a green expertise. *J Adv Res*. 2016;7(1):17–28.
4. Aljawdah HM, Abdel-Gaber R, Al-Shaebi EM, Thagfan FA, Al-Quraishy S, Qasem MA, Murshed M, Mares MM, Al-Otaibi T, Hawsah MA. Hepatoprotective activity of *Eucalyptus camaldulensis* extract in murine malaria mediated by suppression of oxidative and inflammatory processes. *Front Cell Infect Microbiol*. 2022;12: 955042.
5. Ammulu MA, Viswanath KV, Giduturi AK, Vemuri PK, Mangamuri U, Poda S. Phytoassisted synthesis of magnesium oxide nanoparticles from *Pterocarpus marsupium* rox. b heartwood extract and its biomedical applications. *J Genetic Eng Biotechnol*. 2021;19(1):21.
6. Amrulloh H, Fatiqin A, Simanjuntak W, Afriyani H, Annissa A. Antioxidant and antibacterial activities of magnesium oxide nanoparticles prepared using aqueous extract of *Moringa oleifera* bark as green agents. *J Multidiscipl Appl Nat Sci*. 2021.
7. Anigboro AA, Avwioroko OJ, Cholu CO. Phytochemical constituents, antimalarial efficacy, and protective effect of *Eucalyptus camaldulensis* aqueous leaf extract in plasmodium berghei-infected mice. *Preventive Nutr Food Sci*. 2020;25(1):58.
8. Arciniegas-Grijalba P, Patiño-Portela M, Mosquera-Sánchez L, Guerrero-Vargas J, Rodríguez-Páez J. ZnO nanoparticles (ZnO-NPs) and their antifungal activity against coffee fungus *Erythricium salmonicolor*. *Appl Nanosci*. 2017;7(5):225–41.
9. Arsuaga JM, Sotto A, del Rosario G, Martínez A, Molina S, Teli SB, de Abajo J. Influence of the type, size, and distribution of metal oxide particles on the properties of nanocomposite ultrafiltration membranes. *J Membr Sci*. 2013;428:131–41.
10. Avitabile E, Senes N, D'avino C, Tsamesidis I, Pinna A, Medici S, Pantaleo A. The potential antimalarial efficacy of hemocompatible silver nanoparticles from *Artemisia* species against *P. falciparum* parasite. *PLoS ONE*. 2020;15(9):e0238532.
11. Ayalew M, Atnafie SA, Bekele A. Antimalarial activity of solvent fractions of a leaf of *Eucalyptus globulus* labill against *Plasmodium berghei* infected mice. *BMC Complementary Med Ther*. 2022;22(1):221.
12. Baker AN, Hawker-Bond GW, Georgiou PG, Dedola S, Field RA, Gibson MI. Glycosylated gold nanoparticles in point of care diagnostics: From aggregation to lateral flow. *Chem Soc Rev*. 2022;51(16):7238–59.
13. Bedi O, Krishan P. Investigations on acute oral toxicity studies of purpurin by application of OECD guideline 423 in rodents. *Naunyn Schmiedebergs Arch Pharmacol*. 2020;393(4):565–71.
14. Bishwokarma M, Bhujel A, Baskota M, Pandit R. *JNSC*. *J Nepal Chem Soc*. 2021;42(1):45–50.

15. Broglie JJ, Alston B, Yang C, Ma L, Adcock AF, Chen W, Yang L. Antiviral activity of gold/copper sulfide core/shell nanoparticles against human norovirus virus-like particles. *PLoS ONE*. 2015;10(10): e0141050.
16. Chau TP, Kandasamy S, Chinnathambi A, Alahmadi TA, Brindhadevi K. Synthesis of zirconia nanoparticles using *Laurus nobilis* for use as an antimicrobial agent. *Appl Nanosci*. 2023;13(2):1337–44.
17. Djaman JA, Olefongo D, Ako AB, Roman J, Ngane VF, Basco LK, Tahar R. Molecular epidemiology of malaria in Cameroon and Cote d'Ivoire. XXXI. Kelch 13 propeller sequences in *Plasmodium falciparum* isolates before and after implementation of artemisinin-based combination therapy. *Am J Trop Med Hygiene*. 2017;97(1):222.
18. Dkhil MA, Aljawdah HMA, Abdel-Gaber R, Thagfan FA, Delic D, Al-Quraishy S. The effect of *Eucalyptus camaldulensis* leaf extracts from different environmental harvesting locations on *Plasmodium chabaudi*-induced malaria outcome. *Food Sci Technol*. 2023;43: e006723.
19. Ghareeb MA, Habib MR, Mossalem HS, Abdel-Aziz MS. Phytochemical analysis of *Eucalyptus camaldulensis* leaves extracts and testing its antimicrobial and schistosomicidal activities. *Bull Natl Res Centre*. 2018;42:1–9.
20. Haldar K, Bhattacharjee S, Safeukui I. Drug resistance in *Plasmodium*. *Nat Rev Microbiol*. 2018;16(3):156–70.
21. Hanna DH, El-Mazaly MH, Mohamed RR. Synthesis of biodegradable antimicrobial pH-sensitive silver nanocomposites reliant on chitosan and carrageenan derivatives for 5-fluorouracil drug delivery toward HCT116 cancer cells. *Int J Biol Macromol*. 2023;231: 123364.
22. Hassanzadeh-Tabrizi S. Precise calculation of crystallite size of nanomaterials: a review. *J Alloys Compounds*. 171914.
23. Hawadak J, Kojom Foko LP, Pande V, Singh V. In vitro antiplasmodial activity, hemocompatibility and temporal stability of *Azadirachta indica* silver nanoparticles. *Artif Cells Nanomed Biotechnol*. 2022;50(1):286–300.
24. Jagannathan P, Kakuru A. Malaria in 2022: Increasing challenges, cautious optimism. *Nat Commun*. 2022;13(1):1–3.
25. Kabiru Y, Okolie N, Muhammad H, Ogbadoyi E. Preliminary studies on the antiplasmodial potential of aqueous and methanol extracts of *eucalyptus camadulensis* leaf. *Asian Pac J Trop Dis*. 2012;2:S809–14.
26. Kamau E, Campino S, Amenga-Etego L, Drury E, Ishengoma D, Johnson K, Mumba D, Kekre M, Yavo W, Mead D. K13-propeller polymorphisms in *Plasmodium falciparum* parasites from sub-Saharan Africa. *J Infect Dis*. 2015;211(8):1352–5.
27. Khan MI, Akhtar MN, Ashraf N, Najeeb J, Munir H, Awan TI, Tahir MB, Kabli MR. Green synthesis of magnesium oxide nanoparticles using *Dalbergia sissoo* extract for photocatalytic activity and antibacterial efficacy. *Appl Nanosci*. 2020;10:2351–64.
28. Khandel P, Yadav RK, Soni DK, Kanwar L, Shahi SK. Biogenesis of metal nanoparticles and their pharmacological applications: present status and application prospects. *J Nanostruct Chem*. 2018;8(3):217–54.
29. Kojom Foko LP, Eyaane Meva F, Eboumbou Moukoko CE, Ntomba AA, Ngaha Njila MI, Belle Ebanda Kedi P, Ayong L, Lehman LG. A systematic review on anti-malarial drug discovery and antiplasmodial potential of green synthesis mediated metal nanoparticles: overview, challenges and future perspectives. *Malar J*. 2019;18(1):1–14.
30. Kumaresan M, Anand KV, Govindaraju K, Tamilselvan S, Kumar VG. Seaweed *Sargassum wightii* mediated preparation of zirconia (ZrO₂) nanoparticles and their antibacterial activity against gram positive and gram negative bacteria. *Microb Pathog*. 2018;124:311–5.
31. Kumatia EK, Ayertey F, Appiah-Opong R, Bagyour GK, Asare KO, Mbatcho VC, Dabo J. Intervention of standardized ethanol leaf extract of *Annickia polycarpa*, (DC.) Setten and Maas ex IM Turner. (Annonaceae), in *Plasmodium berghei* infested mice produced anti-malaria action and normalized gross hematological indices. *J Ethnopharmacol*. 2021;267:113449.
32. Kwansa-Bentum B, Agyeman K, Larbi-Akor J, Anyigba C, Appiah-Opong R. In vitro assessment of antiplasmodial activity and cytotoxicity of *Polyalthia longifolia* leaf extracts on *Plasmodium falciparum* strain NF54. *Malar Res Treatment*. 2019;2019.
33. Mallmann EJJ, Cunha FA, Castro BN, Maciel AM, Menezes EA, Fechine PBA. Antifungal activity of silver nanoparticles obtained by green synthesis. *Rev Inst Med Trop Sao Paulo*. 2015;57:165–7.
34. Menard S, Tchoufack JN, Maffo CN, Nsango SE, Iriart X, Abate L, Tsapi MT, Awono-Ambéné PH, Abega Mekongo FA, Morlais I. Insight into k13-propeller gene polymorphism and ex vivo DHA-response profiles from Cameroonian isolates. *Malar J*. 2016;15(1):1–7.
35. Misganaw D, Amare GG, Mengistu G. Chemo suppressive and curative potential of *Hypoestes forskalei* against *Plasmodium berghei*: evidence for in vivo antimalarial activity. *J Exp Pharmacol*. 2020;313–323.
36. Mourdikoudis S, Pallares RM, Thanh NT. Characterization techniques for nanoparticles: comparison and complementarity upon studying nanoparticle properties. *Nanoscale*. 2018;10(27):12871–934.
37. Murugan K, Anitha J, Suresh U, Rajaganesh R, Panneerselvam C, Aziz AT, Tseng L-C, Kalimuthu K, Alsali MS, Devanesan S. Chitosan-fabricated Ag nanoparticles and larvivorous fishes: a novel route to control the coastal malaria vector *Anopheles sundaiicus*? *Hydrobiologia*. 2017;797(1):335–50.
38. Najoom S, Fozia F, Ahmad I, Wahab A, Ahmad N, Ullah R, Gul A, Bari A, Khan MY, Khan AA. Effective antiplasmodial and cytotoxic activities of synthesized zinc oxide nanoparticles using *Rhazya stricta* leaf extract. *Evid-Based Complementary Altern Med*. 2021;2021(1):5586740.
39. Narasimha G. Virucidal properties of silver nanoparticles synthesized from white button mushrooms (*Agaricus bisporus*). 2013.
40. Okaiyeto K, Hoppe H, Okoh AI. Plant-based synthesis of silver nanoparticles using aqueous leaf extract of *Salvia officinalis*: characterization and its antiplasmodial activity. *J Cluster Sci*. 2021;32(1):101–9.
41. Parthiban E, Manivannan N, Ramanibai R, Mathivanan N. Green synthesis of silver-nanoparticles from *Annona reticulata* leaves aqueous extract and its mosquito larvicidal and anti-microbial activity on human pathogens. *Biotechnol Rep*. 2019;21: e00297.
42. Patra JK, Baek K-H. Antibacterial activity and synergistic antibacterial potential of biosynthesized silver nanoparticles against food-borne pathogenic bacteria along with its anticandidal and antioxidant effects. *Front Microbiol*. 2017;8:167.
43. Patra JK, Baek KH. Biosynthesis of silver nanoparticles using aqueous extract of silky hairs of corn and investigation of its antibacterial and anticandidal synergistic activity and antioxidant potential. *IET Nanobiotechnol*. 2016;10(5):326–33.
44. Pawar S, Shende P. A comparative outlook on pharmacokinetics and antimalarial studies of artemether and lumefantrine-loaded microneedle patches and a dry suspension containing nanosponges. *J Drug Delivery Sci Technol*. 2020;60: 102055.
45. Roux AT, Maharaj L, Oyegoke O, Akoniyan OP, Adeleke MA, Maharaj R, Okpeku M. Chloroquine and sulfadoxine–pyrimethamine resistance in Sub-Saharan Africa—a review. *Front Genet*. 2021;12: 668574.
46. Ryley J, Peters W. The antimalarial activity of some quinolone esters. *Ann Trop Med Parasitol*. 1970;64(2):209–22.

47. Shayoub MEH, Dawoud ADH, Abdelmageed M, Ehassan AM, Ehassan AM. Phytochemical analysis of leaves extract of *Eucalyptus camaldulensis* Dehnh. 2015.
48. Souleymane D, Abdoulaye AD, Ogobara KD. Methods for monitoring artemisinin-based combination therapies efficacy. *Clin Rev Opinions*. 2017;8(1):1–13.
49. Steketee RW, Choi M, Linn A, Florey L, Murphy M, Panjabi R. World Malaria Day 2021: commemorating 15 years of contribution by the United States president's malaria initiative. *Am J Trop Med Hyg*. 2021;104(6):1955.
50. Su X-Z, Lane KD, Xia L, Sá JM, Wellem's TE. Plasmodium genomics and genetics: new insights into malaria pathogenesis, drug resistance, epidemiology, and evolution. *Clin Microbiol Rev*. 2019. <https://doi.org/10.1128/cmr.00019-00019>.
51. Tran TV, Nguyen DT, Kumar PS, Din AT, Jalil AA, Vo DV. Green synthesis of ZrO₂ nanoparticles and nanocomposites for biomedical and environmental applications: a review. *Environ Chem Lett*. 2022;1–23.
52. Tse EG, Korsik M, Todd MH. The past, present and future of anti-malarial medicines. *Malar J*. 2019;18(1):1–21.
53. Udayabhanu J, Kannan V, Tiwari M, Natesan G, Giovanni B, Perumal V. Nanotitania crystals induced efficient photocatalytic color degradation, antimicrobial and larvicidal activity. *J Photochem Photobiol, B*. 2018;178:496–504.
54. Upadhyay S, Parekh K, Pandey B. Influence of crystallite size on the magnetic properties of Fe₃O₄ nanoparticles. *J Alloy Compd*. 2016;678:478–85.
55. Varadharaj V, Ramaswamy A, Sakthivel R, Subbaiya R, Barabadi H, Chandrasekaran M, Saravanan M. Correction to: antidiabetic and antioxidant activity of green synthesized starch nanoparticles: an in vitro study. *J Cluster Sci*. 2020;31(6):1267–1267.
56. Younis IY, El-Hawary SS, Eldahshan OA, Abdel-Aziz MM, Ali ZY. Green synthesis of magnesium nanoparticles mediated from *Rosa floribunda* charisma extract and its antioxidant, antiaging and antibiofilm activities. *Sci Rep*. 2021;11(1):16868.

Publisher's Note Springer Nature remains neutral with regard to jurisdictional claims in published maps and institutional affiliations.